

Alternated Gravel Mounts With Artificial Assembled Boulders Reinforcement Inside Channelized Rivers

Pietro Beretta Piccoli¹ & Youichi Yasuda²

¹ Department of Civil Engineering, Graduate School of Science and Technology, Nihon University, Tokyo, Japan

² Department of Civil Engineering, College of Science and Technology, Nihon University, Tokyo, Japan

Correspondence: Pietro Beretta Piccoli, PhD student, Civil Engineering Dept., Graduate School of Sci. and Tech., Nihon University, Tower Schola S1010, 1-8-14 Kanda Surugadai, Chiyoda-ku, 101-8308 Tokyo. E-mail: cspi21001@g.nihon-u.ac.jp

Received: May 3, 2023

Accepted: June 1, 2023

Online Published: June 17, 2023

doi:10.20849/jess.v6i1.1352

URL: <https://doi.org/10.20849/jess.v6i1.1352>

Abstract

Alternated gravel mounts are expected to be a simpler and more cost-efficient alternative to traditional river restoration strategies. To improve their stability, two layers of assembled boulders are placed like fallen dominoes facing downstream around the triangular shape of each mount. Further assembled boulders are placed along both sides of the channel. The ecological improvements are quantified by the definition of refuge, i.e. anywhere inside the flow where fishes might escape the flooding's force. In this paper, the needs of small sized fishes are considered (body length under 0.30 m). Point gauge and electrical-magnetic current meter are used to measure elevation and horizontal velocity components, respectively. The channel slope is kept at 0.01, while four different discharges are researched. The collected results are very promising: the introduction of assembled boulders is very important to maintain the model's stability and flatten the water surface along the sides of the channel. The gravel mounts' triangular shape successfully forces the flow to meander. Areas with slow flowing water are generated near the gravel bed along the channel's sides. There, the requirements for the definition of refuge are met. As the water volume increases, the flow straightens, particularly inside the channel's centre, but the refuge able areas are still forming. Each gravel mount is expected to generate a volume suitable for refuge as large as 40% of its own, with limiting factors such as flood's discharge or shallow water conditions having little effect on this performance.

Keywords: alternated mounts, gravel, assembled boulders, refuge areas

1. Introduction

With the aim of improving the poor ecology inside channelized rivers (McRae et al., 2020), the Laboratory for Ecological Hydraulics at the College of Science and Technology, Nihon University, investigates the flow characteristics after arrowhead-shaped gravel mounts are installed on alternating sides of channelized rivers. If successful, the findings would represent a significantly simpler and more cost-efficient option to other, more common, river restoration strategies (Logar et al., 2019).

The initial design (Beretta Piccoli & Yasuda, 2020 and 2021) consisted of arrowhead-shaped mounts with linearly decreasing height from side wall to mount's toe using gravel ($d_{50} = 0.017$ m) as construction material. Beretta Piccoli & Yasuda (2021) settled the best gravel mounts' height at $h_{GM} = 0.044$ m, but they also highlighted the structural instabilities that would turn catastrophic under major flood stages. The second design consisted of rectangular constructions with uniform height using three layers of boulders ($D_{50} = 0.063$ m) assembled on top of each other like fallen dominoes facing downstream. Beretta Piccoli & Yasuda (2022a) highlighted how these more stable structures generate remarkable ecological improvements. At the same time, the steep front and back walls of each construction cause strong hydraulic resistance and the large holes between the assembled boulders increase the seepage flow. It was also discovered that the installation of assembled boulders along the sides of the channel stabilizes the water surface there. The third and final design (Beretta Piccoli & Yasuda 2022b and 2023) consists in combining gravel and assembled boulders as better described in the following chapter.

2. Method

2.1 Experimental Model

The general outlines of the experimental channel have been kept uniform since the first design (Beretta Piccoli & Yasuda, 2020): inside the 15 m long, 0.80 m wide and 0.60 m high rectangular experimental channel, the 5.40 m long model is built using gravel ($d_{50} = 0.017$ m, uniform) to create a $h_{bed} = 0.04$ m thick, flat surface. Beretta Piccoli & Yasuda (2022a) has highlighted the stability benefits of a multi-layered gravel bed. On top of it, seven arrowhead-shaped gravel mounts are installed every 0.80 m on alternated sides of the channel. Each mount has the same characteristics: height $h_{GM} = 0.044$ m above the gravel bed (this value has been selected as the best value in term of hydraulic resistance and ecological improvements in Beretta Piccoli & Yasuda, 2021), transverse length 0.50 m, upstream and downstream width 0.30 m and 0.35 m, respectively. The height linearly decreases from the side wall to the mount's toe. The outline of each mount is reinforced by boulders ($D_{50} = 0.063$ m, uniform) assembled on top of each other in two layers facing downstream. The first downstream stone is inserted inside the gravel bed with a general angle of 20° - 30° from the horizontal. The second is placed over this at a slightly higher angle. The assembled boulders' height follows the mounts' generic outline (i.e. 0.044 m tall at the side of the channel and completely buried inside the gravel bed at the mount's toe). Along both sides of the channel, further two layers of assembled boulders facing downstream are built on the channel's metal surface. The external layer is 0.084 m tall (i.e. in line with the mounts' tops), while the internal one is slightly lower, matching as much as possible the linear reduction of the mounts' outline. The boulders of both layers have a 60° - 70° angle from the horizontal. A metal bar is placed at the downstream end of each model to improve its stability. The installation area is shown in Figure 1.

The upstream end of the model is defined as the origin of the x-axis with positive direction toward downstream, while the centre of the channel is chosen as the origin of the y-axis with positive direction on the left in flow direction. The metal surface of the experimental channel has an elevation of $z = 0$ m. Under these definitions, $x = 5.40$ m is the downstream end of the model; the right and left side walls have $y = -0.40$ m and $y = 0.40$ m, respectively. Elevation is measured using a point gauge with 1 mm sensitivity. For the gravel bed, data are collected every 0.1 m (0.05 m when above a gravel mount) in x-direction for $0 \leq x$ (m) ≤ 5.40 and $y = -0.38, -0.30, -0.20, -0.10, 0, 0.10, 0.20, 0.30, 0.38$ m. The water surface is measured in the same fashion, but only in centre and sides of the channel ($y = 0, \pm 0.30$ m for Case 1 and Case 2; $y = 0, \pm 0.38$ m for Case 3 and Case 4). An I-type probe electrical-magnetic current meter KENEK CO. model VM-806H/VMT2-200-04P with ± 0.005 m/s sensitivity, sampling frequency 20 Hz and measurement time 30 s for a total 601 point-values measurements (KENEK information sheet) is used to collect the longitudinal (x-direction) and lateral (y-direction) velocity components. Data are collected inside two separate flow regions: $1.10 \leq x$ (m) ≤ 3.20 and $y = 0, 0.10, 0.20, 0.38$ m, as well as $1.90 \leq x$ (m) ≤ 4.00 and $y = -0.38, -0.20, -0.10, 0$ m. For Case1 and Case2, measurements are taken at $y = \pm 0.3$ m instead of $y = \pm 0.38$ m because the assembled boulders emerge above the water surface. The channel slope is fixed at $I = 0.01$ (i.e. 1%), as Beretta Piccoli & Yasuda (2021) highlighted that the changes in the hydraulic conditions are more significant here than above smoother slopes. Four different discharges are chosen to investigate the changes in the flow conditions around the installed gravel mounts: $Q = 3.7 \times 10^{-3}$ m³/s and $Q = 5.5 \times 10^{-3}$ m³/s represents two small-sized flooding events; $Q = 59 \times 10^{-3}$ m³/s (Beretta Piccoli & Yasuda, 2023) is considered medium-size level, while $Q = 155 \times 10^{-3}$ m³/s (Beretta Piccoli & Yasuda, 2022b and 2023) is the maximal capacity of the experimental channel.



Figure 1. (left, a) gravel mount is viewed from downstream; (right, b) model is shown from downstream

2.2 Mathematical Formulas

The average water depth h_{ave} [m] is calculated from the average water elevation z_{ave} [m] (collected data) minus the bottom thickness $h_{bed} = 0.04$ m. Only the measurements inside the quasi-uniform flow are used (i.e. free from up- or downstream boundary effects). The Froude number is calculated from the average water depth, the channel's width $B = 0.8$ m and the gravitational acceleration constant $g = 9.81$ m/s².

$$Fr = \frac{Q}{B \cdot h_{ave} \cdot \sqrt{h_{ave} \cdot g}} \quad (1)$$

For each measurement, the total flow velocity U_{TOT} [m/s] is found by the vectorial sum of the two horizontal components measured with the current meter: longitudinal u [m/s] and lateral v [m/s]. Each measurement is comprised of $n = 601$ point-values. Useful for this research are the time-averaged velocity $\overline{U_{TOT}}$ [m/s] and the standard deviation of the velocity $std(U_{TOT})$ [m/s].

$$\overline{U_{TOT}} = \frac{1}{n} \cdot \sum_{i=1}^n U_{TOT,i} \quad (2a)$$

$$std(U_{TOT}) = \sqrt{\frac{\sum_{i=1}^n (U_{TOT,i} - \overline{U_{TOT}})^2}{n}} \quad (2b)$$

The ecological improvements are quantified by the definition of “refuge able areas”, i.e. anywhere inside the flow area where suitable conditions allow small sized fishes to escape the main flow's force. Following literature research and experiments using living fishes and a scaled gravel model (Beretta Piccoli & Yasuda 2020), suitable swimming conditions are defined by two acceptable upper limits: $\overline{U_{TOT}} \leq 0.10$ m/s and $std(U_{TOT}) \leq 0.07$ m/s. Small sized fishes are defined as having a body length smaller than 0.30 m. Ayu Sweetfishes (*Plecoglossus altivelis*) are used as flagbearers of the category and they have most of the cited literature research focuses on them (Nakamura et al. 1995; Onitsuka et al., 2005 and 2009). Here also studied are the requirements of Formosan landlocked salmons (*Oncorhynchus masou formosanus*, Lin et al., 2006), longfin eels (*Anguilla dieffenbachia*, Graynoth & Booker, 2009) and coral reef fishes (*alichoeres margaritaceus*, *Pomacentrus chrysurus* and *Chrysiptera brownriggi*, Johnsen et al. 2007 and 2008).

Further suitable regions are expected to be found in the void interstices between the assembled boulders (Beretta Piccoli & Yasuda 2020 and 2022a). These regions are defined as “refuge areas” A_R [m²] and comprise of 30% of the total volume of an assembled boulder construction (Beretta Piccoli & Yasuda, 2022a).

Vertical velocity profiles can be constructed putting together all measurements taken at same (x,y)-coordinates. Using polynomial approximation (1st, 2nd or 4th depending on accuracy and number of available points), it is possible to simulate a continuous velocity profile from the gravel bed to the water surface. The height of the refuge able area h_{RA} [m] at the given coordinates is found as the maximal elevation above the gravel bed where the defined thresholds for refuge are found. When the vertical velocity profile never reaches these thresholds, $h_{RA} = 0$ m. For each studied y-coordinate, the refuge able area A_{RA} [m²] is found as:

$$A_{RA,y} = \sum \left(\frac{h_{RA,x} + h_{RA,x+\Delta x}}{2} \cdot \Delta x \right) \quad (3)$$

Δx , Δy are the distances between two measurements along the x- or y-axis, respectively ($\Delta x = 0.10$ m always, while $\Delta y = 0.10$ m or 0.08 m). The total refuge able volume V_{RA} [m³] is found as the sum of the refuge able areas:

$$V_{RA} = \sum \left(\frac{A_{RA,y} + A_{RA,y+\Delta y}}{2} \cdot \Delta y \right) \quad (4)$$

The area of the gravel mount A_{GM} [m²] is calculated using the same method. The height of the mount l_{GM} [m] at given coordinates is the elevation of the gravel surface above the bottom thickness $h_{bed} = 0.04$ m. The letter “ l_{GM} ” is here used to differentiate this variable from the height of the gravel mounts $h_{GM} = 0.044$ m.

$$A_{GM,y} = \sum \left(\frac{l_{GM,x} + l_{GM,x+\Delta x}}{2} \cdot \Delta x \right) \quad (5)$$

Because a combination of gravel and assembled boulders are used to build the gravel mounts, the ratio between mount’s volume V_{GM} [m³] and refuge volume V_R [m³] must be calculated differently depending on the y-coordinate. Along the sides of the channel ($0.3 < |y|$ (m) ≤ 0.38) and the centre ($y = 0$ m), the mounts’ profile is composed only by assembled boulders. Therefore, 70% of the total volume there is considered part of V_{GM} , the rest part of V_R . At the coordinates in-between ($y = \pm 0.10, \pm 0.20$ m), the area of gravel A_{gra} [m²] and assembled boulders A_{sb} [m²] are worked separately. The two are separated using the sinks at both sides of each mount’s profile as border. At $y = \pm 0.3$ m, A_{gra} and A_{sb} are estimated by polynomial approximation 1st grade using the known areas as reference points (at $y = 0$ m, $A_{gra} = 0$ m², while A_{sb} must be halved since each channel’s side is considered separately). The areas are then added to find the volumes. The gravel volume is entirely considered part of V_{GM} , as well as 70% of the assembled boulders’ volume. The remaining 30% is part of V_R , as explained earlier. Equation (4) is used to calculate both V_{GM} and V_R , changing A_{RA} with the sum ($A_{gra}+A_{sb}$).

3. Results

3.1 Gravel Stability

The gravel mounts remain stable under all the tested discharges. Under the largest discharge ($Q = 155 \times 10^{-3}$ m³/s, Case 4), gravel shaking is widespread with some local transport observed in the top area of each mount, where the grains are most exposed. In contrast, assembled boulders always remain motionless. The results are a significant improvement from the previous designs, thanks primarily to the introduction of assembled boulders reinforcements along the shape of each mount (as shown in Beretta Piccoli & Yasuda 2022b).

3.2 Average Water Depth and Froude Number

The average water depth h_{ave} [m] and the Froude number Fr [-] are shown for each case in Table 2. Both parameters grow with discharge and the average water depth in Case 1 and Case 2 is smaller than 0.044 m, the height of both the gravel mounts and the assembled boulders built along the channel’ sides. The flow conditions change from subcritical flow ($Fr < 1$) in Case 1, Case 2 and Case 3, to supercritical flow ($Fr > 1$) in Case 4.

Table 2. Average water depth and Froude number in relationship to each case’s discharge.

	Q [m ³ /s]	h_{ave} [m]	Fr [-]
Case 1	3.7×10^{-3}	0.035	0.23
Case 2	5.5×10^{-3}	0.039	0.29
Case 3	59×10^{-3}	0.111	0.64
Case 4	155×10^{-3}	0.145	1.15

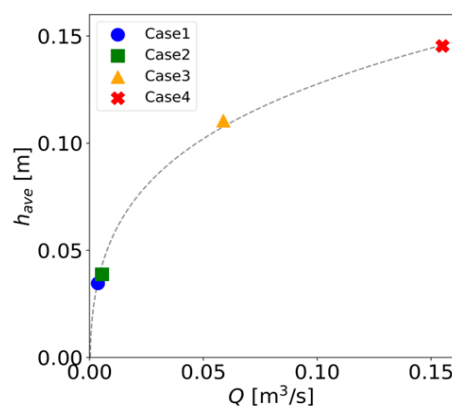


Figure 2. The relationship between discharge and average water depth is shown. The trend is represented with a 4th grade polynomial fit (grey dotted curve).

The rise of the average water surface in relationship with discharge is plotted in Figure 2. As shown, the growth curve can be accurately approximated with a polynomial fit of 4th grade. The relationship between Froude number and discharge has a very similar shape. It is therefore possible to estimate that critical flow conditions (i.e. $Fr = 1$) should be reached around $Q \cong 130 \times 10^{-3}$ m³/s.

3.3 Water Surface Profile

Figure 3 shows the water surface profile inside the quasi-uniform area for each case. As described in the previous section, the water level increases with discharge. Waves are formed, most clearly in the central area of the channel. As highlighted in Beretta Piccoli & Yasuda (2022a and 2022b), the assembled boulders built along the sides of the channel are very important in keeping the water profile flat there. Figure 3 confirms that this effect is maintained even in the case of large discharges. As described previously, the average water depth in Case 1 and Case 2 is lower than the height of the assembled boulders along the sides. Even if the measurements are taken at $y = \pm 0.30$ m, some of the rocks emerge from the water surface profiles of Figure 3a and Figure 3b. Thanks to the polynomial approximation function presented in Figure 2, it is possible to estimate that all assembled boulders should be fully submerged for $Q \geq 5.8 \times 10^{-3} \text{ m}^3/\text{s}$, i.e. slightly above Case 2's tested discharge.

3.4 Meandering Behaviour

For each case, flow intensity and direction inside the measurement area are presented in Figure 4 to Figure 7. Each time, (a) presents the measurement elevation closest to the gravel bed, while (b) the one closest to the water surface.

The pictures confirm that the installation of alternated gravel mounts successfully forces the flow to meander, increasing both the lateral and the longitudinal flow heterogeneity. Behind each gravel mount, areas with significantly slower flow velocity are observed. Previous research has highlighted how these regions meet suitable swimming conditions for small sized fishes (Beretta Piccoli & Yasuda 2020 and 2021). Based on these observations, refuge able areas appear to form under all researched discharges and their size to remain generally constant with increasing flow volume. The intensity of the meander appears the strongest near the gravel bed surface when the discharge is small (Figure 4a, Case 1). By the increase of measurement elevation and/or discharge, the flow straightens (Figure 6, Case 3 and Figure 7, Case 4). The measurements in Figure 6b and Figure 7b are very similar to what would be observed inside a channelized river with flat gravel bed.

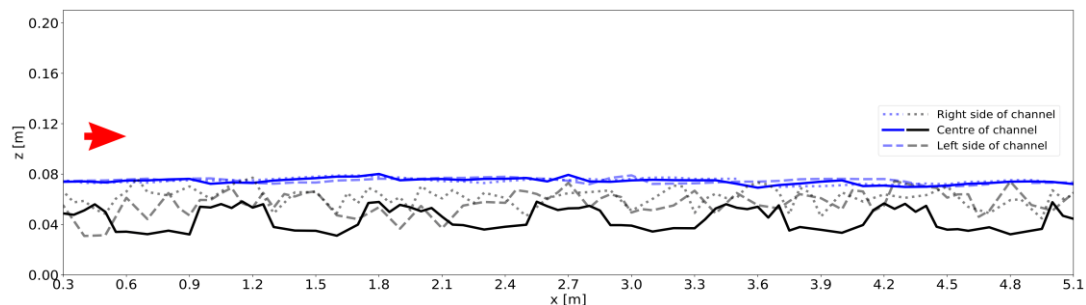


Figure 3a. Water surface profile for Case 1 ($Q = 3.7 \times 10^{-3} \text{ m}^3/\text{s}$). Colour blue is used for water, black for the gravel mounts. Continuous lines represent the centre of the channel, while the dotted ones the sides ($y = \pm 0.30$ m). Flow direction is given by the red arrow.

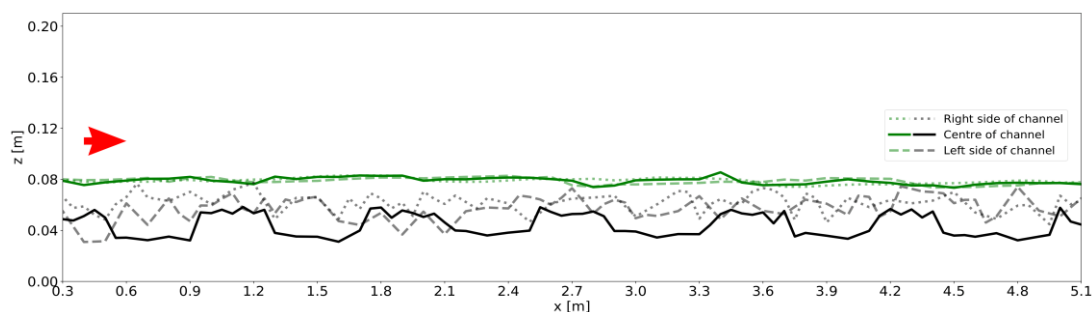


Figure 3b. Water surface profile for Case 2 ($Q = 5.5 \times 10^{-3} \text{ m}^3/\text{s}$). Colour green is used for water, black for the gravel mounts. Continuous lines represent the centre of the channel, while the dotted ones the sides ($y = \pm 0.30$ m). Flow direction is given by the red arrow.

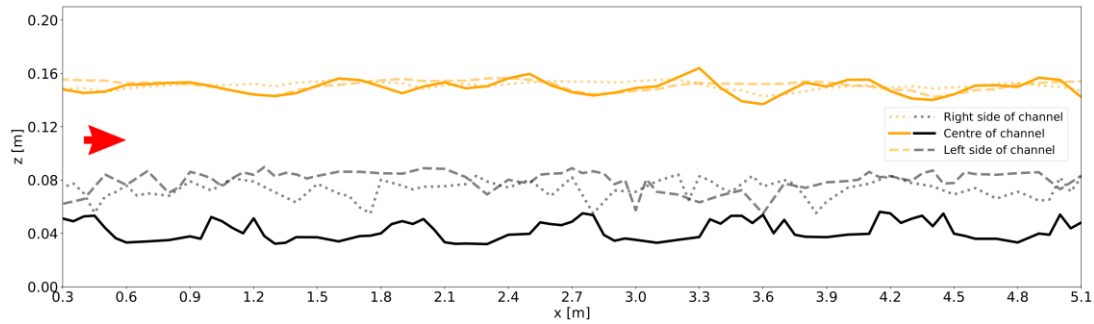


Figure 3c. Water surface profile for Case 3 ($Q = 59 \times 10^{-3} \text{ m}^3/\text{s}$). Colour orange is used for water, black for the gravel mounts. Continuous lines represent the centre of the channel, while the dotted ones the sides ($y = \pm 0.38 \text{ m}$). Flow direction is given by the red arrow.

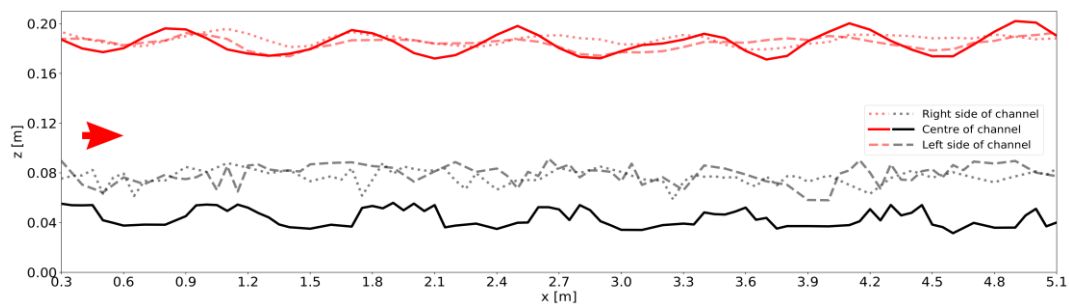


Figure 3d. Water surface profile for Case 4 ($Q = 155 \times 10^{-3} \text{ m}^3/\text{s}$). Colour red is used for water, black for the gravel mounts. Continuous lines represent the centre of the channel, while the dotted ones the sides ($y = \pm 0.38 \text{ m}$). Flow direction is given by the red arrow.

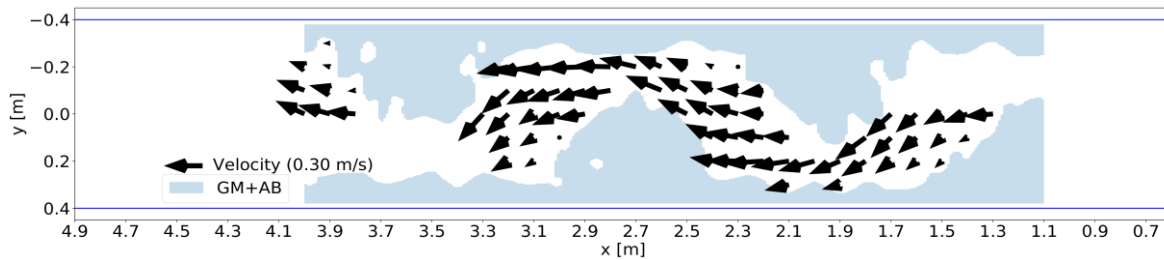


Figure 4a. Meandering behaviour for Case 1 ($Q = 3.7 \times 10^{-3} \text{ m}^3/\text{s}$) at elevation $z-h_{\text{bed}} = 0.01 \text{ m}$ (close to the gravel bed). Flow velocity and direction are given by the black arrows scaled to the plot's axis (legend for reference). The blue area represents the combined surface of gravel and assembled boulders (hence “GM+AB”).

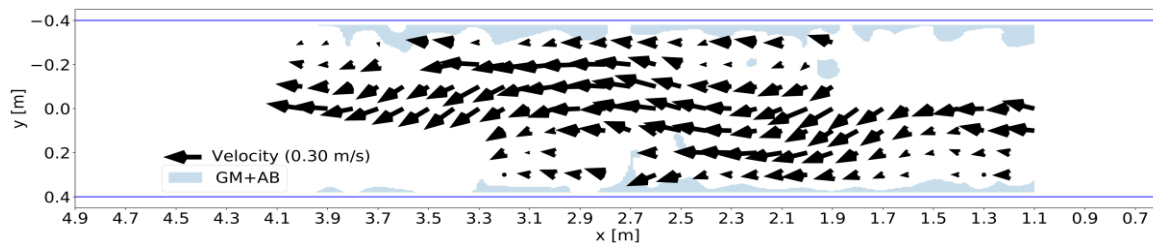


Figure 4b. Meandering behaviour for Case 1 ($Q = 3.7 \times 10^{-3} \text{ m}^3/\text{s}$) at elevation $z-h_{\text{bed}} = 0.03 \text{ m}$ (close to the water surface). Flow velocity and direction are given by the black arrows scaled to the plot's axis (legend for reference). The blue area represents the combined surface of gravel and assembled boulders (hence “GM+AB”).

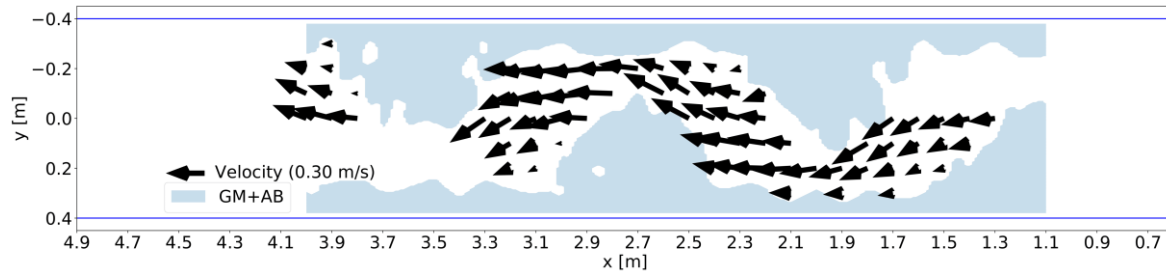


Figure 5a. Meandering behaviour for Case 2 ($Q = 5.5 \times 10^{-3} \text{ m}^3/\text{s}$) at elevation $z-h_{\text{bed}} = 0.01 \text{ m}$ (close to the gravel bed). Flow velocity and direction are given by the black arrows scaled to the plot's axis (legend for reference). The blue area represents the combined surface of gravel and assembled boulders (hence "GM+AB").

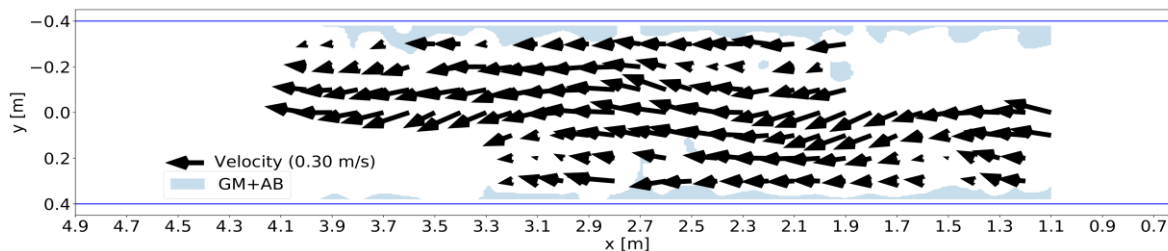


Figure 5b. Meandering behaviour for Case 2 ($Q = 5.5 \times 10^{-3} \text{ m}^3/\text{s}$) at elevation $z-h_{\text{bed}} = 0.03 \text{ m}$ (close to the water surface). Flow velocity and direction are given by the black arrows scaled to the plot's axis (legend for reference). The blue area represents the combined surface of gravel and assembled boulders (hence "GM+AB").

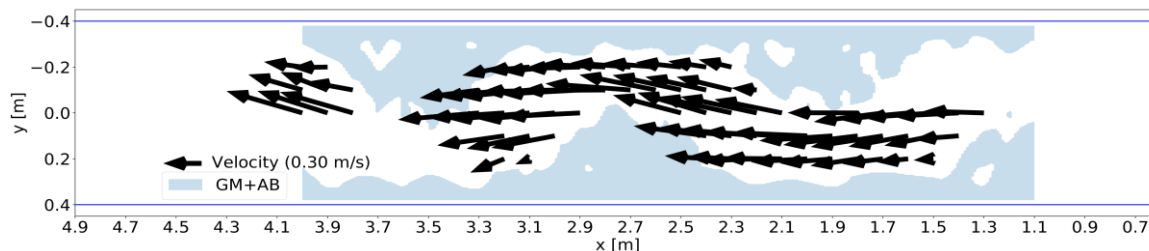


Figure 6a. Meandering behaviour for Case 3 ($Q = 59 \times 10^{-3} \text{ m}^3/\text{s}$) at elevation $z-h_{\text{bed}} = 0.01 \text{ m}$ (close to the gravel bed). Flow velocity and direction are given by the black arrows scaled to the plot's axis (legend for reference). The blue area represents the combined surface of gravel and assembled boulders (hence "GM+AB"). This plot has been presented once before in Beretta Piccoli and Yasuda (2023).

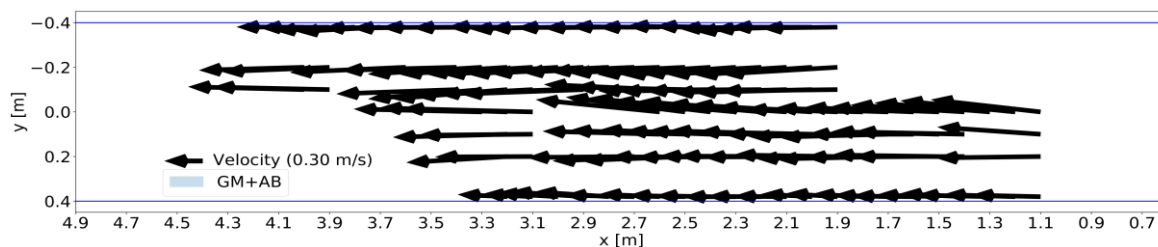


Figure 6b. Meandering behaviour for Case 3 ($Q = 59 \times 10^{-3} \text{ m}^3/\text{s}$) at elevation $z-h_{\text{bed}} = 0.08 \text{ m}$ (close to the water surface). Flow velocity and direction are given by the black arrows scaled to the plot's axis (legend for reference). The blue area represents the combined surface of gravel and assembled boulders (hence "GM+AB"). This plot has been presented once before in Beretta Piccoli and Yasuda (2023).

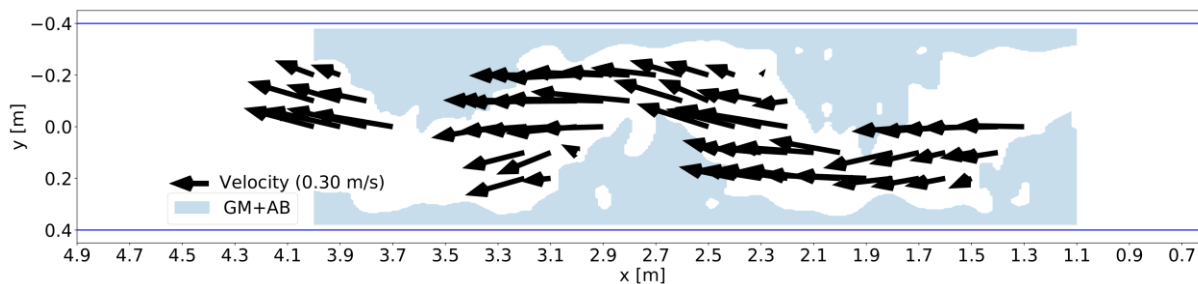


Figure 7a. Meandering behaviour for Case 4 ($Q = 155 \times 10^{-3} \text{ m}^3/\text{s}$) at elevation $z-h_{\text{bed}} = 0.01 \text{ m}$ (close to the gravel bed). Flow velocity and direction are given by the black arrows scaled to the plot's axis (legend for reference). The blue area represents the combined surface of gravel and assembled boulders (hence "GM+AB").

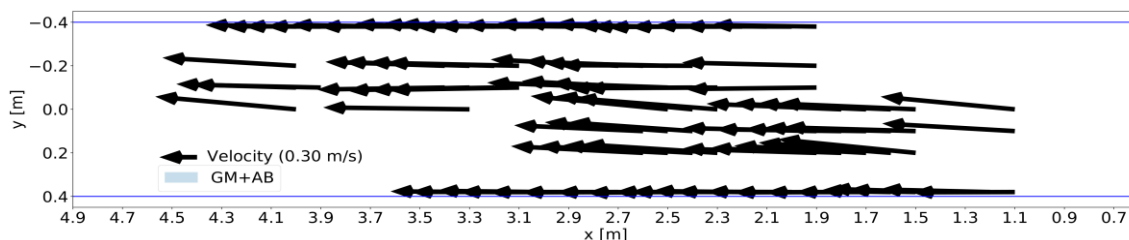


Figure 7b. Meandering behaviour for Case 4 ($Q = 155 \times 10^{-3} \text{ m}^3/\text{s}$) at elevation $z-h_{\text{bed}} = 0.10 \text{ m}$ (close to the water surface). Flow velocity and direction are given by the black arrows scaled to the plot's axis (legend for reference). The blue area represents the combined surface of gravel and assembled boulders (hence "GM+AB").

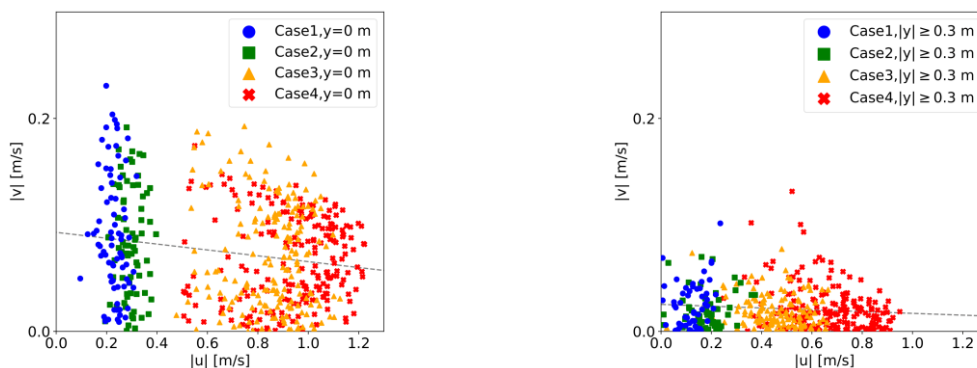


Figure 8. Measurements are sorted by position: channel's centre on the left (a), sides on the right (b). Velocity components u (x -direction) and v (y -direction) are plotted in absolute value. The trend is given by the gray line.

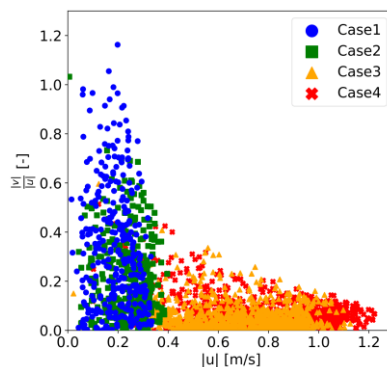


Figure 9. The ratio between the absolute value of both velocity components expresses the meandering behaviour. This is plotted against the absolute value of u .

Figure 8 confirms that the flow straightens with increasing discharge. As the grey trend line is significantly steeper in Figure 8a than Figure 8b, the straightening behaviour appears to affect more the centre of the channel ($y = 0$ m) rather than the sides ($|y| \geq 0.3$ m). In Figure 9, the meandering behaviour of the flow is shown by plotting the ratio of the absolute value of both velocity components. The data emulate an exponential negative function, as small discharges change little but are very noticeable ($Q = 3.7 \times 10^{-3} \text{ m}^3/\text{s}$ to $5.5 \times 10^{-3} \text{ m}^3/\text{s}$) and large discharges are very different but makes almost no impact in the plot ($Q = 59 \times 10^{-3} \text{ m}^3/\text{s}$ to $155 \times 10^{-3} \text{ m}^3/\text{s}$).

3.5 Gravel Mount Volume, Refuge Volume and Refuge Able Volume

The refuge able volume V_{RA} , the refuge volume V_R and the mounts volume V_{GM} are shown for each case in Table 3 (the results for Case 3 have been presented in Beretta Piccoli and Yasuda, 2023). For Case 1 and Case 2, only the mounts' volume under the average water depth is taken into consideration. Because the same plan is used for all models, V_{GM} (and V_R which is directly related to it) remains almost constant. More importantly, the total refuge able volume appears to remain stable despite the increasing discharge between cases. On average, V_R takes up 23% of the total space occupied by each gravel mount. This is a smaller percentage than the 30% measured for constructions made solely by assembled boulders (Beretta Piccoli & Yasuda, 2022a). The relative refuge volume is expressed by the sum of V_{RA} and V_R divided by V_{GM} . The lowest value is calculated in Case 1 (37%), where the shallow water is considered the main limiting factor for the creation of refuge (able) areas. The large discharges in Case 3 and Case 4 do not appear to hinder the model's performance as the relative refuge volume remains constant at 40%. Somewhere between Case 2 and Case 3, the optimal discharge is expected to be placed, where the balance between sufficiently deep water and not too large flow velocity is met. From the results shown in Table 3, each gravel mount is expected to generate suitable refuge volumes around 40% of its own, independently from the discharge.

Table 3. Gravel mount, refuge and refuge able volumes, as well as relative refuge volume, are shown for each case.

	$V_{GM} [10^{-3} \text{ m}^3]$	$V_R [10^{-3} \text{ m}^3]$	$V_{RA} [10^{-3} \text{ m}^3]$	$(V_R + V_{RA})/V_{GM} [-]$
Case 1	14.20	4.18	1.15	0.37
Case 2	14.60	4.34	1.76	0.42
Case 3	14.10	4.24	1.33	0.40
Case 4	14.80	4.39	1.57	0.40

4. Conclusions

The installation of alternated gravel mounts with assembled boulders reinforcements along their shape and the sides of the channelized river has shown very promising results. The model stability is guaranteed even under stress of the maximal capacity of the experimental channel. This is almost entirely due to the strength of assembled boulders constructions which also play an important role in flattening the water surface along the channel's sides. The triangular shape of each gravel mounts forces the flow to meander, thus increasing the local flow heterogeneity. This is most visible near the gravel surface under small discharges. By increasing the water volume, the flow tends to straighten, particularly around the centre of the channel, although the meandering behaviour is still visible. Behind each gravel mount, areas with slow flowing water are found where the suitable conditions for refuge for small sized fishes are met. These regions are shown to remain in place in both shallow water and high discharge conditions. Results suggest that each gravel mount can generate a volume suitable for refuge around 40% its own.

Future research should focus on exiting the laboratory conditions in favor of more prototype-oriented experiments. It is important to understand if the proposed model is equally effective inside real channelized rivers. The biological study could expand to comprehend spawning and/or other aquatic species (e.g. medium and large sized fishes, microorganisms). Finally, the conditions should be investigated when the gravel mounts are no longer stable (i.e. the assembled boulders are moved). This would settle the applicability ranges of the proposed bed morphology.

References

- Beretta, P. P., & Yasuda, Y. (2021). Formation of refuge areas behind alternative gravel dikes for fishes during flood stages. *Modern Environmental Science and Engineering Journal*, (11), 1021-1031). Academic Star Publishing. [https://doi.org/10.15341/mese\(2333-2581\)](https://doi.org/10.15341/mese(2333-2581))
- Beretta, P. P., & Yasuda, Y. (2022a). Experimental analysis on the formation of refuge areas for fishes behind alternative gravel dikes in channelized rivers during flood stages. *Proceedings of the 39th IAHR World Congress* (pp. 2290-2299). <https://doi.org/10.3850/IAHR-39WC252171192022679>
- Beretta, P. P., & Yasuda, Y. (2022b). Experimental analysis on the stability of alternative gravel dikes during flood stages in channelized rivers, to be published in *the Proceedings of the 11th International Conference on Fluvial Hydraulics, River Flow 2022*.
- Beretta, P. P., & Yasuda, Y. (2023). Formation of refuge able areas around different gravel mounts' designs, to be presented at *the 40th IAHR World Congress 2023 and to be published in its Proceedings*.
- Beretta, P. P., Yasuda, Y., & Boes, R. (2020). Installation of alternative gravel mounts in channelized rivers. *Proceedings of the 22nd IAHR-ADP Congress 2020*.
- Graynoth, E., & Booker, D. (2009). *Biomass of longfin eels in medium to large rivers*. New Zealand Fisheries Assessment Report 2009/44.
- Johansen, J. L., Fulton, C. J., & Bellwood, D. R. (1972). Coral reef fishes exploit flow refuges in high-flow habitats. *Marine Ecology Progress Series*, 360, 219-226. <https://doi.org/10.3354/meps07482>
- Johansen, J. L., Fulton, C. J., & Bellwood, D. R. (2007). Avoiding the flow: refuges expand the swimming potential of coral reef fishes. *Coral Reefs*, 26, 577-583. Springer Verlag. <https://doi.org/10.1007/s00338-007-0217-y>
- KENEK CO. LDT. (no date). Multiple channel types Electro-magnetic Current Meter, product information sheet. Model VM-806H/VMT2-400-04P.
- Lin, J.-Y., Chen, Y.-C., Tsao, E. H., & Yang, H.-C. (2006). Reformation of Formosan Landlocked Salmon habitat as refuge during high flows. *Doboku Gakkai Ronbunshuu B*, 62(4), 320-329.
- Logar, I., Brouwer, R., & Paillex, A. (2019). Do the societal benefits of river restoration outweigh their costs? A cost-benefit analysis. *Journal of Environmental Management*, 232, 1075-1085.
- McRae, L., Deinet, S., Marconi, V., Scott-Gatty, K., & Freeman, R. (2020). *A deep drive into freshwater, Living Planet Report 2020*. WWF – World Wide Fund for Nature.
- Nakamura, S., Ishikawa, M., Tsukisaka, M., Azuma, N., & Nakamura, Y. (1995). Field research to obtain the IFIM's preference curves for Japanese fresh water fishes. *Proceedings of The 2nd Symposium on River Channel Hydraulics and the River Environment*, pp. 127-134.
- Onitsuka, K., Nagaya, T., Higashino, M., Takami, T., Otsuka, N., Akiyama, J., ... Shiraishi, Y. (2005). Study on suitable hydraulic condition for spawning and living of ayu. *Collection of Academic Theses*, 4, 1471-1476.
- Onitsuka, K., Nagaya, T., Shiraishi, Y., Ukese, A., Higashino, M., Takami, T., ... Serikawa, T. (2009). *A Proposal of Preference Curves of Velocity for Ayu*. Kyushu Institute of Technology.

Copyrights

Copyright for this article is retained by the author(s), with first publication rights granted to the journal.

This is an open-access article distributed under the terms and conditions of the Creative Commons Attribution license (<http://creativecommons.org/licenses/by/4.0/>).